J. Fluid Mech. (1972), *vol.* 54, *part* 3, *pp.* 495–506
Printed in Great Britain

A similarity solution for viscous internal waves

By N. H. THOMAS AND T. N. STEVENSON
Department of the Mechanics of Fluids, University of Manchester

(Received 19 January 1972)

A similarity solution is presented which describes the internal waves generated by a simple-harmonic localized disturbance in a stably stratified viscous fluid. Some experimental results support the theoretical predictions for the waves in a linearly stratified salt solution.

1. Introduction

The internal wave system generated by a small simple-harmonic disturbance in a density-stratified inviscid non-diffusive liquid has been investigated by Görtler (1943) and Mowbray & Rarity (1967). Their shadow and schlieren photographs of the phase configuration of the waves in a uniformly stratified salt solution confirmed the fundamental result of the linear theory. This predicts that, for wavelengths small compared with the scale height of the stratification, waves of frequency ω propagate in a fluid of natural frequency ω_0 along straight lines inclined at the angle $\sin^{-1}(\omega/\omega_0)$ to the horizontal.

This paper describes some theoretical and experimental studies of the two-dimensional wave system in a viscous fluid. It is shown that the governing equations yield a perturbation similarity solution when written in a co-ordinate system stationary relative to the undisturbed fluid, with the origin near the disturbance and with axes parallel to the group velocity and phase velocity vectors in the inviscid wave solution. Apart from an unsteady term the final equation resembles the integral form, given by Janowitz (1968), of Long's (1962) solution for the far-field flow generated by a two-dimensional body moving horizontally in a linearly stratified viscous diffusive fluid.

2. Similarity solution

A horizontal two-dimensional body oscillates with frequency ω in an unbounded density-stratified viscous incompressible non-diffusive fluid. The mean position of the body is near the origin of a Cartesian co-ordinate system Ox_0y_0, which is stationary relative to the undisturbed fluid, with y_0 measured vertically upwards (see figure 1(*b*), plate 1). An exponential distribution of mean density, $\rho_0 = \rho^* \exp(-\beta y_0)$, implies constant natural frequency $\omega_0 = (g\beta)^{\frac{1}{2}}$, where g is the acceleration due to gravity and ρ^* and β are constants. A second co-ordinate system is defined by the relations $x' = x_0 \cos\theta + y_0 \sin\theta$, $y' = x_0 \sin\theta - y_0 \cos\theta$, where θ is the angle between the Ox' axis and the horizontal and is given by the dispersion relation $\sin\theta = \omega/\omega_0$ for steady-state small amplitude internal waves

of short wavelength. The left-handed co-ordinate system is chosen so that Ox' and Oy' are parallel to the group velocity and phase velocity vectors of the inviscid waves (see figure 1(*b*), plate 1). The velocity components are u' and v', the density is ρ_T, μ_T is the viscosity p_T the pressure and t' is the time. The perturbation variables $p' = p_T - p_0$, $\rho' = \rho_T - \rho_0$ and $\mu' = \mu_T - \mu_0$ are introduced, μ_0 and p_0 being the equilibrium values. The equations of continuity and incompressibility are

$$\frac{\partial u'}{\partial x'} + \frac{\partial v'}{\partial y'} = 0 \tag{1}$$

and

$$\frac{\partial \rho'}{\partial t'} + u' \frac{\partial \rho_T}{\partial x'} + v' \frac{\partial \rho_T}{\partial y'} = 0, \tag{2}$$

and the perturbation momentum equations obtained by subtracting the hydrostatic relations are

$$\rho_T\left(\frac{\partial u'}{\partial t'} + u' \frac{\partial u'}{\partial x'} + v' \frac{\partial u'}{\partial y'}\right) = -\frac{\partial p'}{\partial x'} + 2\frac{\partial}{\partial x'}\left(\mu_T \frac{\partial u'}{\partial x'}\right) + \frac{\partial}{\partial y'}\left[\mu_T\left(\frac{\partial u'}{\partial y'} + \frac{\partial v'}{\partial x'}\right)\right] - \rho' g \sin\theta \tag{3}$$

and

$$\rho_T\left(\frac{\partial v'}{\partial t'} + u' \frac{\partial v'}{\partial x'} + v' \frac{\partial v'}{\partial y'}\right) = -\frac{\partial p'}{\partial y'} + 2\frac{\partial}{\partial y'}\left(\mu_T \frac{\partial v'}{\partial y'}\right) + \frac{\partial}{\partial x'}\left[\mu_T\left(\frac{\partial u'}{\partial y'} + \frac{\partial v'}{\partial x'}\right)\right] + \rho' g \cos\theta. \tag{4}$$

The boundary conditions are

$$u', v', p', \rho' \to 0 \quad \text{as} \quad y' \to \pm\infty.$$

The variables are now rendered dimensionless in the following way:

$$t' = t(\omega_0 \sin\theta)^{-1}, \quad x' = x(\beta \sin\theta)^{-1}, \quad y' = y\alpha(\beta \sin\theta)^{-1}, \quad \rho' = \rho a \rho^*,$$

$$u' = uag\omega_0^{-1}, \quad v' = v\alpha ag\omega_0^{-1}, \quad \mu' = \mu a \mu^*, \quad p' = p\alpha a \rho^* g(\beta \tan\theta)^{-1},$$

where $$\alpha = [(\omega_0^3 \nu^*/2g^2)\tan\theta \sin\theta]^{\frac{1}{3}}, \quad \nu^* = \mu^*/\rho^*.$$

μ^* is the equilibrium viscosity at the horizontal level of the origin and a is a constant amplitude coefficient.

Experiments show that the energy propagating from the disturbance is confined to a narrow region centred on the line $y = 0$. This can be seen in the schlieren photograph in figure 1(*a*) (plate 1). Measurements described in the next section show that the velocity is essentially parallel to the y axis. The solution is therefore sought under a boundary-layer type of approximation in which perturbations in the x direction are assumed small compared with those in the y direction. It is assumed that $\alpha \ll 1$, that the amplitude of oscillation is small, such that $a \ll \alpha$, and that θ is not near 0 or $\frac{1}{2}\pi$. The implications of these approximations will be discussed later.

Equations (1)–(4) reduce to

$$\frac{\partial u}{\partial x} + \frac{\partial v}{\partial y} = 0, \tag{5}$$

$$\frac{\partial \rho}{\partial t} = r_0(u - \alpha v \cot\theta), \tag{6}$$

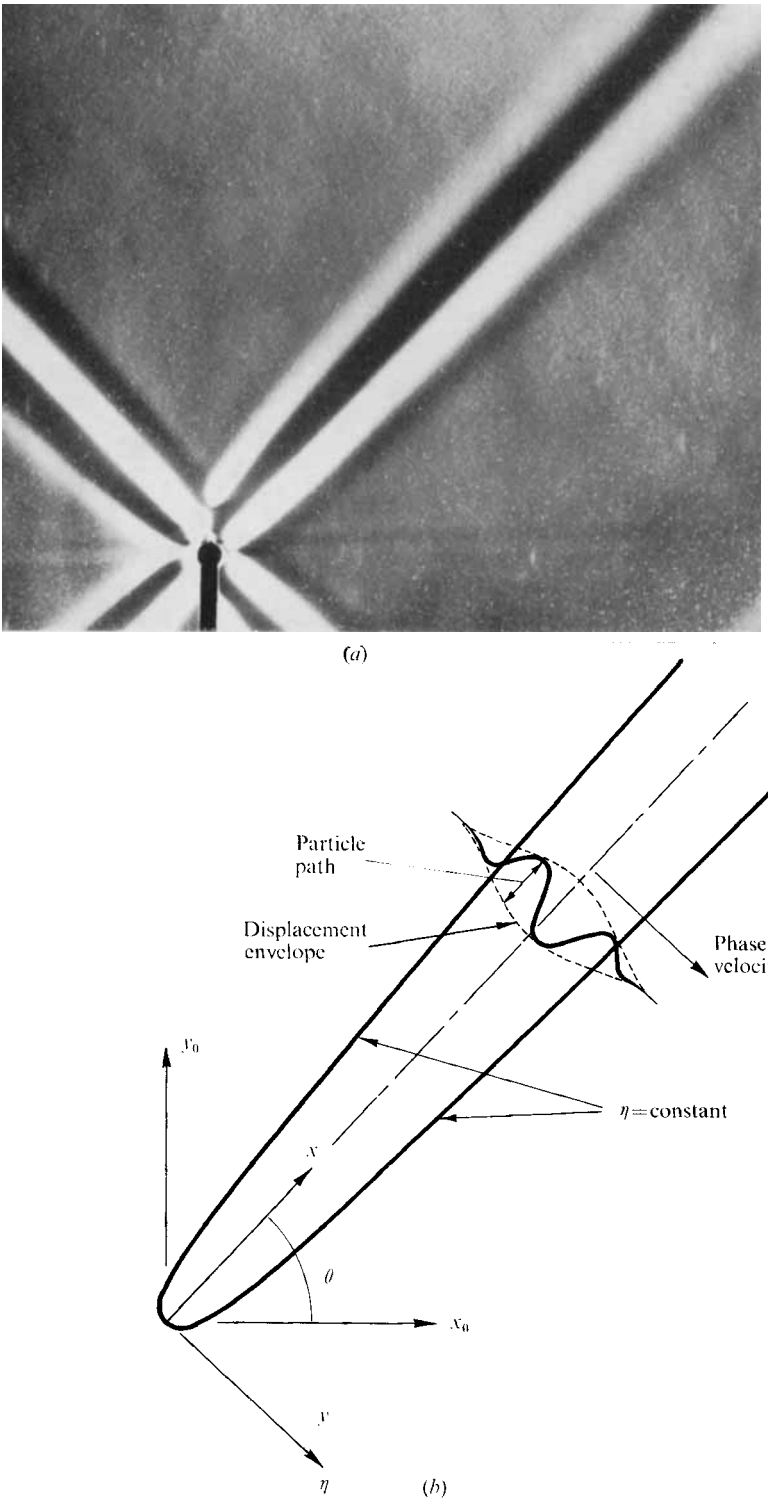

FIGURE 1. (*a*) Schlieren photograph of an internal wave. The photograph is taken looking through the side of the tank and the black vertical line is the cylinder support. (*b*) Diagram of the co-ordinate axes, the phase velocity and the particle displacements in the wave.

$$r_0\frac{\partial u}{\partial t} = -\rho + \alpha\cot\theta\left\{-\frac{\partial p}{\partial x} + 2\frac{\partial}{\partial y}\left(\gamma_0\frac{\partial u}{\partial y}\right) + O(\alpha^2)\right\}, \tag{7}$$

$$\frac{\partial p}{\partial y} = \rho - r_0\alpha\tan\theta\frac{\partial v}{\partial t} + O(\alpha^2), \tag{8}$$

where $r_0 = \rho_0/\rho^* = r_1(x) + \alpha r_2(x,y) + O(\alpha^2)$ with $r_1 = \exp(-x)$ and $r_2 = y\cot\theta\exp(-x)$. $\gamma_0 = \mu_0/\mu^*$ and is assumed to be of the form

$$\gamma_0 = \gamma_1(x) + \alpha\gamma_2(x,y) + O(\alpha^2).$$

The boundary conditions are $u, v, p, \rho \to 0$ as $y \to \pm\infty$.

It is assumed that the perturbation variables have a time dependency e^{-it} and may be expanded as

$$u = u_1 + \alpha u_2 + \ldots, \quad v = v_1 + \alpha v_2 + \ldots,$$
$$p = p_1 + \alpha p_2 + \ldots, \quad \rho = \rho_1 + \alpha\rho_2 + \ldots.$$

These series are substituted into (5)–(8) and terms of like order are equated to give

$$\rho_1 = ir_1u_1 = \partial p_1/\partial y, \tag{9}$$

$$\rho_2 = i\{r_1(u_2 - v_1\cot\theta) + r_2u_1\}, \tag{10}$$

$$r_1u_2 + r_2u_1 = -i\rho_2 + i\cot\theta\left(-\frac{\partial p_1}{\partial x} + 2\gamma_1\frac{\partial^2 u_1}{\partial y^2}\right), \tag{11}$$

$$\partial p_2/\partial y = \rho_2 + ir_1v_1\tan\theta, \tag{12}$$

$$r_1v_1 = i(\partial p_1/\partial x + p_1). \tag{13}$$

ρ_2 and u_2 are eliminated between (10) and (11) and the resulting equation is written in terms of p_1:

$$\frac{\gamma_1}{r_1}\frac{\partial^3(p_1r_1^{-\frac{1}{2}})}{\partial y^3} - i\frac{\partial(p_1r_1^{-\frac{1}{2}})}{\partial x} = 0. \tag{14}$$

This equation may be integrated across the wave to yield

$$r_1^{-\frac{1}{2}}\int_{-\infty}^{\infty} p_1\,dy = J\,e^{-it},$$

where J is a dimensionless constant which is proportional to the momentum flux. Equation (14) may be written as

$$\frac{\partial^3(p_1r_1^{-\frac{1}{2}})}{\partial y^3} - i\frac{\partial(p_1r_1^{-\frac{1}{2}})}{\partial X} = 0, \tag{15}$$

where $X = \int_0^x \nu_1(\bar{x})\,d\bar{x}$ with $\nu_1 = \gamma_1/r_1$.

A solution of the form $p_1r_1^{-\frac{1}{2}} = Re\{X^{-\frac{1}{3}}f(\eta)\,e^{-it}\}$,

where $\eta = y/X^{\frac{1}{3}}$, satisfies the momentum integral equation and yields the ordinary differential equation

$$3f''' + i(\eta f' + f) = 0, \tag{16}$$

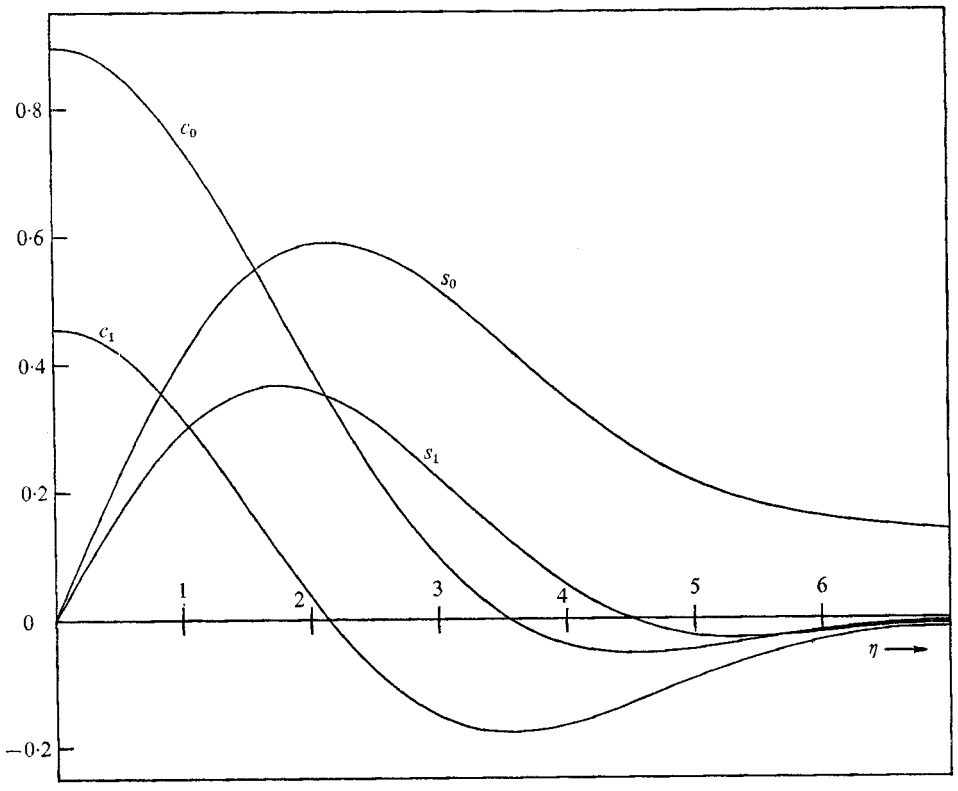

FIGURE 2. The functions $c_0(\eta), c_1(\eta), s_0(\eta)$ and $s_1(\eta)$.

which has the integral solution

$$f = \int_0^\infty \exp(-K^3)\exp(iK\eta)\,dK. \tag{17}$$

If the real functions $c_m(\eta)$ and $s_m(\eta)$ are defined by the relation

$$c_m + is_m = \int_0^\infty K^m \exp(-K^3)\exp(iK\eta)\,dK,$$

then the dimensionless variables have the following solutions:

$$p_1 r_1^{-\frac{1}{2}} = X^{-\frac{1}{3}}(c_0\cos t + s_0\sin t), \tag{18}$$

$$u_1 r_1^{\frac{1}{2}} = X^{-\frac{2}{3}}(c_1\cos t + s_1\sin t), \tag{19}$$

$$v_1 r_1^{\frac{1}{2}} = X^{-\frac{4}{3}}(-c_3\sin t + s_3\cos t) + \tfrac{1}{2}X^{-\frac{1}{3}}(-c_0\sin t + s_0\cos t). \tag{20}$$

Under the Boussinesq approximation r_1 would be unity, X would be replaced by x, and the last term in (20) would be absent.

The functions c_m and s_m when $m > 2$ may be expressed in terms of c_0, c_1, s_0 and s_1, which are shown in figure 2. As s_0 is an odd function it makes no contribution to the dimensionless momentum flux, and

$$J = 2\int_0^\infty c_0\,d\eta = \pi$$

by Fourier's integral theorem.

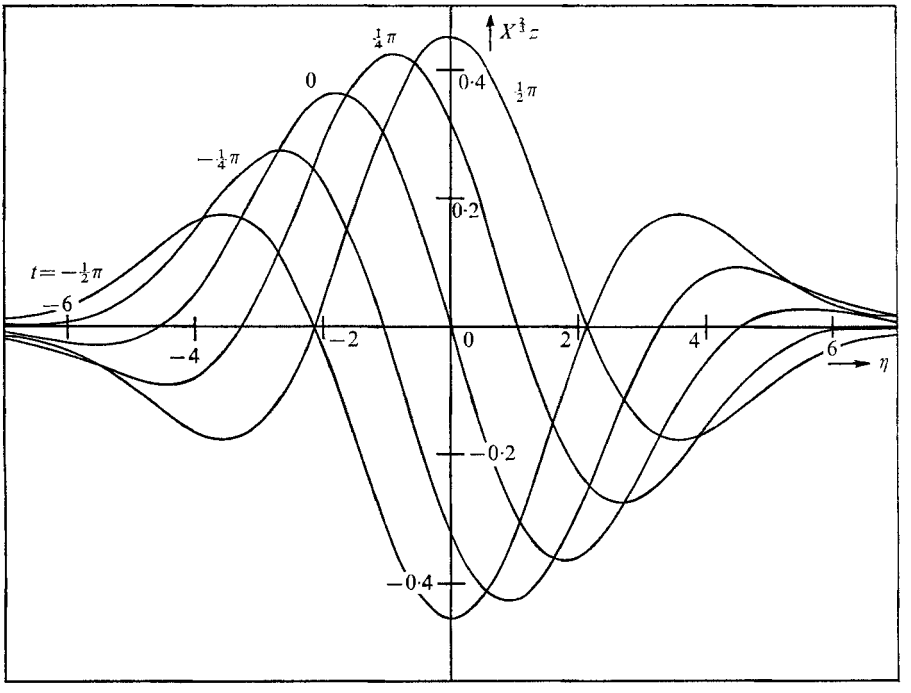

FIGURE 3. The similarity displacement profiles.

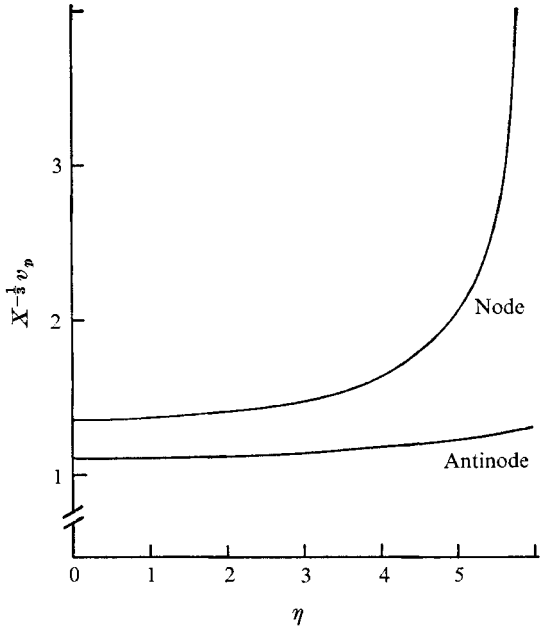

FIGURE 4. The phase velocity of the nodes and antinodes.

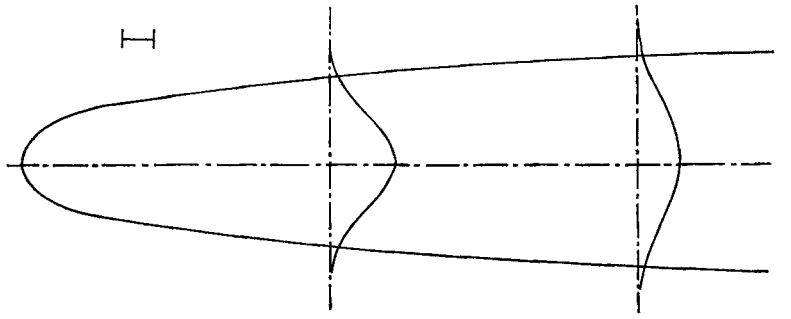

FIGURE 5. The rate of spread of the internal wave. The edge of the ray, given by $|\eta| = \eta^*$, is plotted in the co-ordinate system (Ax', Ay'), where $A = (2\nu^{*-1}\omega_0 \cos\theta)^{\frac{1}{3}}$. The displacement envelope $a\hat{z}$ is shown for values of $Ax' = 100$ and 200. The scale mark represents 10 units of distance and $\frac{1}{100}$ unit of amplitude. ν_0 is constant.

Most of the discussion is couched in terms of the particle displacements ξ parallel to the Ox axis. To the order of the solution, the dimensionless displacement, $z = \xi a^{-1}\beta \sin\theta$, is given by

$$z = X^{-\frac{2}{3}} r_1^{-\frac{1}{2}} \{c_1 \sin t - s_1 \cos t\}. \tag{21}$$

Figure 3 shows the similarity displacement profile at several values of t. The points of constant phase move in the direction of increasing η, that is, towards the horizontal level of the disturbance, at a rate which depends on both the position and the phase. For example, the nodes and the antinodes, the points at which $c_1 \sin t - s_1 \cos t = 0$ and $c_2 \cos t + s_2 \sin t = 0$, have dimensionless phase velocities, $v_p = X^{\frac{1}{3}} \partial\eta/\partial t$, given by

$$v_p = X^{\frac{1}{3}} E_1^2 (c_1 c_2 + s_1 s_2)^{-1}$$

and

$$v_p = X^{\frac{1}{3}} E_2^2 (c_2 c_3 + s_2 s_3)^{-1},$$

where $E_m(\eta) = (c_m^2 + s_m^2)^{\frac{1}{2}}$ is the envelope. These functions are presented in figure 4.

The locus of points of constant η is given by

$$y' = \eta\,(x'\nu^*/2\omega_0 \cos\theta)^{\frac{1}{3}}. \tag{22}$$

The wave width increases indefinitely as θ approaches $\frac{1}{2}\pi$ and tends to a finite limit as θ tends to zero. However the conditions under which the solution is valid are outlined in appendix A, where it is shown that the boundary-layer approximation fails near these limits. The inviscid solution with the perturbations confined to the Ox axis is recovered in the limit $\nu^* \to 0$.

The rate of spread of the band containing the energy and the attenuation of the particle displacements is illustrated in figure 5. This shows the locus (22) evaluated at $|\eta| = \eta^*$ and some examples of the envelope $\hat{z}$ of the particle displacements. η^* is the value of η for which $E_1(\eta^*)/E_1(0) = 0{\cdot}1$. When ν_1 is constant the variation in amplitude $\hat{z}_{\max}$ with distance along the ray is given by

$$\hat{z}_{\max}/E_1(0) = (\beta y_0)^{-\frac{2}{3}} \exp(\tfrac{1}{2}\beta y_0).$$

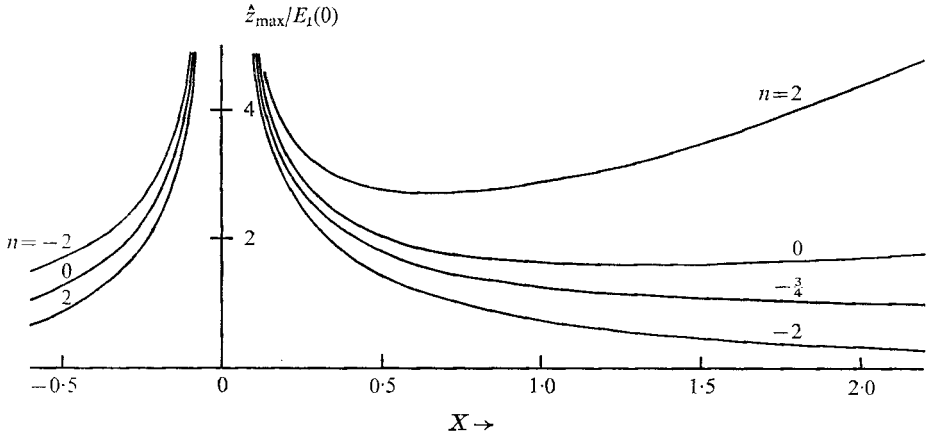

FIGURE 6. The effects of viscosity stratification on the maximum displacements along the centre of the wave.

The amplitude attenuates with increasing depth and initially decreases with increasing altitude, reaching a minimum value at $\beta y_0 = \frac{4}{3}$, after which it increases, eventually leading to an exponential breakdown in the linear approximation. The linear approximation also fails near the disturbance (see appendix A).

The effects of variations in the background viscosity may be estimated by assuming a simple power law relation between viscosity and density: $\nu_1 = r_1^n$. For values of $n \neq 0$ this yields $X = (1/n)[1-\exp(-nx)]$, and the amplitude variation is given by

$$\hat{z}_{\max}/E_1(0) = |(1/n)[1-\exp(-nx)]^{-\frac{3}{4}}\exp(-\tfrac{1}{2}x)|.$$

Some examples of this function are presented in figure 6, which also shows the case $n = 0$ discussed earlier. A decrease in ν_0 (i.e. $n \gtrless 0$ as $x \gtrless 0$) results in a decrease in the wave width and an increase in the wave amplitude, such that the balance between the viscous shear and the pressure force is maintained. As far as the linear approximation is concerned, the critical value of n is $-\frac{3}{4}$, when $\hat{z}_{\max}/E_1(0)$ asymptotes to $(\frac{3}{4})^{\frac{3}{4}}$ as $x \rightarrow +\infty$. The wave amplifies or attenuates as $x \rightarrow +\infty$ depending on whether $n \gtrless -\frac{3}{4}$ and attenuates as $x \rightarrow -\infty$.

Thomas (1971) has considered the case of an isothermal atmosphere, which corresponds to the incompressible solution for $n = -1$ with the wave width and the wave amplitude increased by the factor $[\gamma/(\gamma-1)]^{\frac{3}{4}}$, where γ is the ratio of the specific heats. In view of the above results it is concluded that the waves decay with increasing altitude. Thomas has also shown that the solution can accommodate thermal and solute diffusion in liquids.

3. Experiments

A circular cylinder was mounted in a water tank which was filled with a constant gradient stratified salt solution. A sketch of the apparatus is shown in Mowbray & Rarity (1967). A small electric motor forced the model to oscillate normal to its longitudinal axis. The model was positioned to yield the maximum length of ray before interception by waves reflected from the walls of the tank.

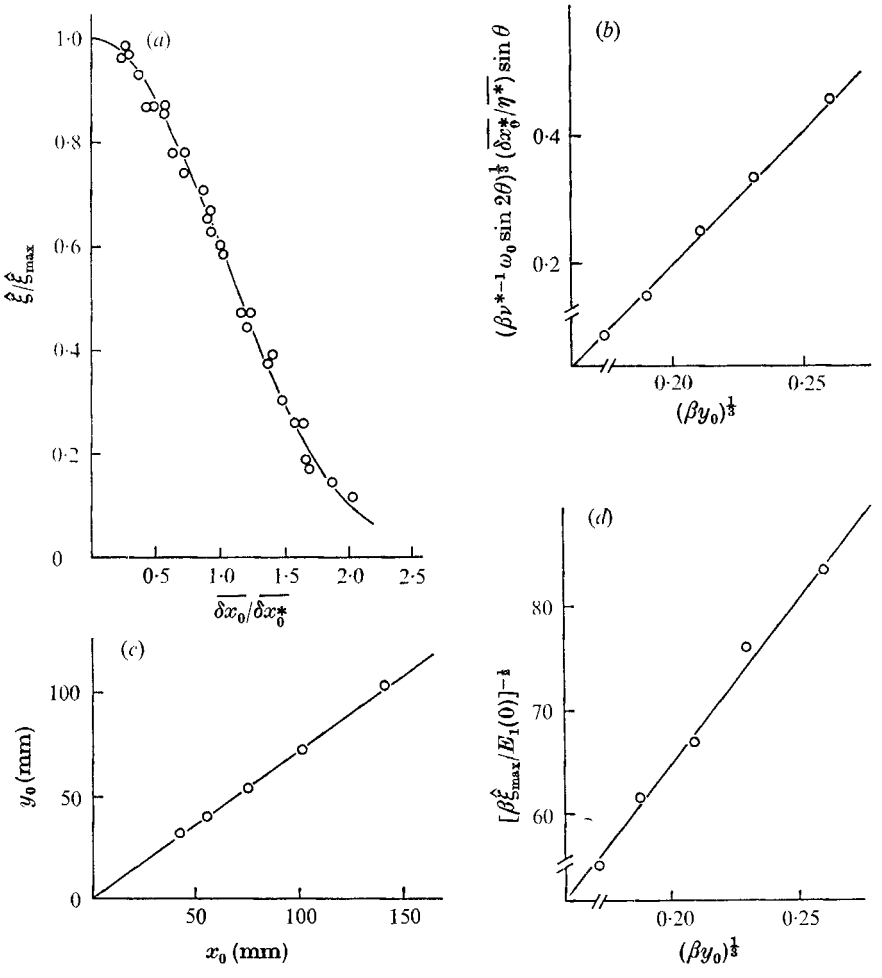

FIGURE 7. Particle displacement measurements for a 9·5 mm diameter cylinder oscillating horizontally with a period of 8·3 s and an amplitude of 3·0 mm. (*a*) The mean displacement envelopes compared with the similarity profile. (*b*) The wave width variation with altitude. (*c*) The ray path. (*d*) The attenuation rate. The straight lines are from the theory.

A travelling microscope was used to measure the displacement of neutrally buoyant oil drops formed from a mixture of di-ethyl pthalate ($\rho = 1{\cdot}12\,\mathrm{g\,cm^{-3}}$) and mesitylene ($\rho = 0{\cdot}86\,\mathrm{g\,cm^{-3}}$). The model amplitude was adjusted to produce particle displacements which were typically 0·5 mm and therefore large compared with the diameter of the oil drops, about 0·02 mm, and the accuracy ($\pm$ 0·01 mm) of measuring their displacement. The major source of experimental error was the level of the general disturbance, about 0·05 mm, produced by the reflected waves and the oscillating viscous mixing layer at the level of the body.

The region in which measurements were taken was small compared with the stratification height β^{-1} so the experimental results can be reasonably compared with the solution of the Boussinesq equations. The maximum displacements, $\hat{\xi}$, were recorded at particular points in the ray during a series of horizontal traverses,

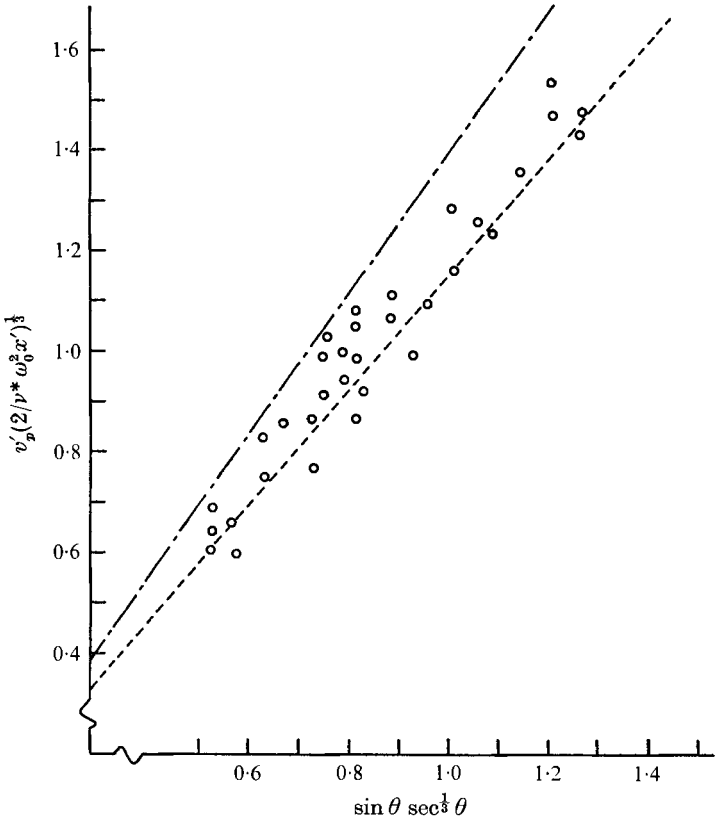

FIGURE 8. Phase velocity measurements compared with the theoretical nodal and antinodal phase velocities. ———, node; – – – –, antinode.

which, with the flow visualization technique employed, were more convenient than traverses normal to the ray path. In figure 7 (*a*) $\xi/\xi_{\max}$ is plotted against $\overline{\delta x_0}/\overline{\delta x_0^*}$, where $2\overline{\delta x_0}$ is the horizontal distance between points with the same ξ, and $2\overline{\delta x_0^*}$ is the value of $2\overline{\delta x_0}$ for which $\xi/\xi_{\max} = 0{\cdot}6$. The validity of making this comparison is discussed in appendix B. The agreement between theory and experiment is good. The variation across the ray of the inclination of the particle paths to the horizontal was greater than predicted by the theory and was possibly due to the general disturbance produced by the body.

Theoretically the variation of $\overline{\delta x_0^*}$ with altitude is given approximately by the equations (see appendix B)

$$(\beta\nu^{*-1}\omega_0 \sin 2\theta)^{\frac{1}{3}}(\overline{\delta x_0^*}/\overline{\eta}^*)\sin\theta = (\beta y_0)^{\frac{1}{3}}; \quad E_1(\overline{\eta}^*)/E_1(0) = 0{\cdot}6. \tag{23}$$

This is compared with the experimental results in figure 7 (*b*), in which the altitude is measured from the position at which the ray appears to originate, the virtual origin. The linearity of the plot gives support to the choice of similarity variable.

The linear density distribution produces an inhomogeneity with respect to ω_0, causing the ray path to bend slightly towards the horizontal. The effect is negligible over the range of altitudes used in the experiment as can be seen from

figure 7 (*c*), which compares the co-ordinates of the maximum displacement $\hat{\xi}_{\max}$ with the theoretical ray path.

The experimental values of $[\beta\hat{\xi}_{\max}/E_1(0)]^{-\frac{1}{2}}$ versus $(\beta y_0)^{\frac{1}{3}}$ are shown in figure 7 (*d*). The linear plot supports the theoretical attenuation rate. Equating the measured slope with the theoretical value of $a^{-\frac{1}{2}}\cos\theta$ we obtain $a \simeq 7\times10^{-6}$. In the theory it was assumed that $a \ll \alpha$, and as α is approximately 2×10^{-3} in the experiments a is two orders of magnitude less than α.

The dimensional phase velocity v_p' is given by

$$v_p' = x^{-\frac{1}{3}}\, v_p(\tfrac{1}{2}\omega_0^2\nu^*x')^{\frac{1}{3}}\sec^{\frac{1}{3}}\theta\sin\theta. \tag{24}$$

Figure 4 shows that, near the centre of the wave, the dimensionless phase velocity v_p is approximately $1{\cdot}4x^{\frac{1}{3}}$ for the nodes and $1{\cdot}15x^{\frac{1}{3}}$ for the antinodes. The antinodal phase velocities were estimated from the schlieren image by timing the movement of the boundary between the light and dark regions at various positions in the wave. In figure 8 the measurements are shown to compare quite well with the theory.

4. Conclusions

Experimental results in a linearly stratified salt solution support the main features of the theoretical solution for viscous internal waves. Maximum displacements, attenuation rates and phase velocity all compare quite well with the theory but no time-dependent displacement profiles have been measured.

Acknowledgement is made to the Ministry of Technology, who supported this work. N. H. Thomas was in receipt of a Science Research Council maintenance grant.

Appendix A

An estimate of the error introduced by neglecting the nonlinear terms is obtained from the momentum integral equation, which takes the form

$$\int_{-\infty}^{\infty}(r_1^{-\frac{1}{2}}p_1 + a\alpha^{-1}u^2\tan\theta)\,dy \simeq J e^{-it}.$$

The error, estimated from the temporal root-mean-square (r.m.s.) contribution of the nonlinear term to the r.m.s. momentum flux, is less than 10 % when

$$\frac{2^{\frac{3}{2}}a}{J\alpha}\left(\int_0^{\infty}u^2\,dy\right)_{\text{r.m.s.}}\tan\theta < 0{\cdot}1$$

or, after evaluating the integral using the first-order solution and inverting the condition, when

$$|x| > 2{\cdot}5a\alpha^{-1}\tan\theta. \tag{25}$$

The boundary-layer approximation should be reasonable when

$$\alpha|v/u|\,(\cot\theta, \tan\theta) < 0{\cdot}1 \tag{26}$$

and

$$\tfrac{1}{2}\alpha|y|\cot\theta < 0{\cdot}1. \tag{27}$$

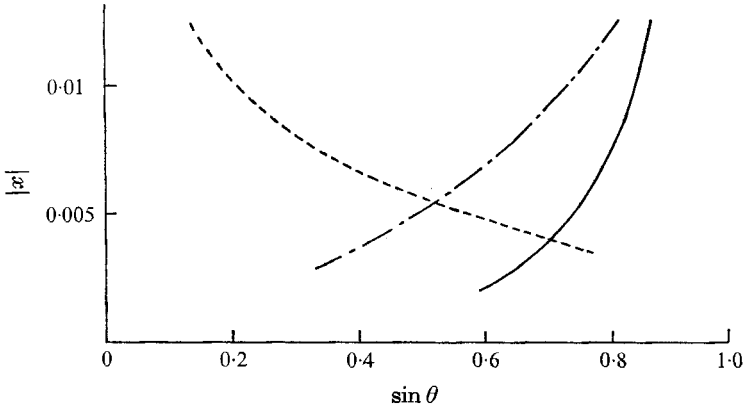

FIGURE 9. Validity of the similarity solution when $a = 10^{-5}\sin\theta$ and $\alpha^3 = 10^{-8}\tan\theta\sin\theta$. ------, $46\alpha^{\frac{3}{2}}\cot^{\frac{3}{2}}\theta$; — — — —, $2{\cdot}5\alpha^{-1}\tan\theta$; ———, $46\alpha^{\frac{3}{2}}\tan^{\frac{3}{2}}\theta$. The boundaries represent the lower limits of $|x|$ for which the solution is valid.

The magnitude of $|v/u|$ may be estimated from

$$v_{\text{r.m.s.}}/u_{\text{r.m.s.}} = |x|^{-\frac{2}{3}}E_3/E_1 + \tfrac{1}{2}|x|^{\frac{1}{3}}E_0/E_1.$$

The last term will dominate at large $|x|$ but the conditions (26) and (27) would be satisfied when $|x| < 10^3$ for the present experimental values of α. The maximum value of E_3/E_1 is 1·28 and $E_0/E_1 \simeq |\eta|$ at large $|\eta|$, so conditions (26) and (27) may be written as $1{\cdot}28\alpha|x|^{-\frac{2}{3}}(\tan\theta, \cot\theta) < 0{\cdot}1$ and $\frac{1}{2}\alpha|y|\,(\tan\theta, \cot\theta) < 0{\cdot}1$. The second pair of conditions is satisfied when $|y| \leqslant y_B$, say, so the integral constraint must be truncated at $|y| = y_B = \eta_B|x|^{\frac{1}{3}}$. The truncation error $2J^{-1}\int_{\eta_B}^{\infty} c_0\,d\eta$ is less than 10% when $\eta_B > \eta^* = 5{\cdot}85$, or when $3\alpha|x|^{\frac{1}{3}}(\tan\theta, \cot\theta) < 0{\cdot}1$. For values of $|x| < 0{\cdot}43$ this is less restrictive than the first pair of conditions, which inverts to

$$|x| > 46\alpha^{\frac{3}{2}}(\tan^{\frac{3}{2}}\theta, \cot^{\frac{3}{2}}\theta). \tag{28}$$

The boundaries of $|x|$ implied by (25) and (28) are shown in figure 9 for typical laboratory values of α and a. For the present experiments the largest error in the similarity solution is approximately 10% and occurs for the lowest altitude traverse.

Appendix B

The particle displacements were measured at various positions on a horizontal plane. If the horizontal traverse crosses the x' axis at x_1' then a point in the traverse is given by

$$(x', y') = (x_1'(1+\epsilon), \delta x\sin\theta),$$

where $\epsilon x_1' = \delta x_0\cos\theta$ and δx_0 is the horizontal co-ordinate measured from x_1'. Equation (22) may be written as

$$\delta x_0(1+\epsilon)^{-\frac{1}{3}} = \kappa\eta, \quad \text{where} \quad \kappa = (\nu^* y_0/\omega_0\sin 2\theta)^{\frac{1}{3}}\operatorname{cosec}\theta.$$

κ is constant for each horizontal traverse. The similarity envelope is given by

$$E_1(\eta)/E_1(0) = (1+\epsilon)^{\frac{3}{2}}\,\hat{\xi}/\hat{\xi}_{\max}.$$

If the local co-ordinates of the two points with equal values of $\hat{\xi}$ are δx_0^+ and $-\delta x_0^-$ with the corresponding ϵ and η values ϵ^+ and $-\epsilon^-$ and η^+ and $-\eta^-$, and if the mean values are indicated by bars, i.e.

$$\overline{\delta x_0} = \tfrac{1}{2}(\delta x_0^+ + \delta x_0^-),$$

then expansion of the $1+\epsilon$ terms yields

$$\overline{\delta x_0}[1-\tfrac{1}{3}(\epsilon^+-\epsilon^-)+O(\bar{\epsilon}^2)] = \kappa\bar{\eta}$$

and

$$E_1(\bar{\eta})/E_1(0) = (\hat{\xi}/\hat{\xi}_{\max})[1+\tfrac{1}{3}(\epsilon^+-\epsilon^-)+O(\bar{\epsilon}^2)].$$

Under the experimental conditions, an error of less than 5 % is introduced when these expressions are truncated to $\overline{\delta x_0} = \kappa\eta$ and $E_1(\bar{\eta})/E_1(0) = \hat{\xi}/\hat{\xi}_{\max}$.

REFERENCES

Görtler, H. 1943 *Z. angew. Math. Mech.* **23**, 65.

Janowitz, G. S. 1968 *J. Fluid Mech.* **33**, 417.

Long, R. R. 1962 *J. Hydraulics Div., A.S.C.E.* **88**, 9.

Mowbray, D. E. & Rarity, B. S. H. 1967 *J. Fluid Mech.* **28**, 1.

Thomas, N. H. 1971 Ph.D. thesis, University of Manchester.